Computation of Solid/Liquid Phase Change Including Free Convection—Comparison with Data

G. E. Schneider*
University of Waterloo, Waterloo, Ontario, Canada

A computational model is presented for solid/liquid phase-change energy transport including free convection fluid flow in the liquid phase. The computational model considers the velocity components of all nonliquid control volumes to be zero but fully solves the coupled mass-momentum problem within the liquid. The thermal energy model includes the entire domain and employs an enthalpy-like model and a recently developed method for handling the phase-change interface nonlinearity. Convergence studies are performed and comparisons made with experimental data for two different problems. Grid independence is achieved, and the comparison with experimental data indicates excellent quantitative prediction of the melt fraction evolution. Qualitative data are also provided as velocity vector and isotherm plots. The computational costs incurred are quite low by comparison with other models.

Nomenclature

A = finite-difference coefficients
b = right side
C = transient coefficient
c = specific heat
e = specific energy
Fo = Fourier modulus
g = gravitational acceleration
H = half height of domain
h = enthalpy
k = thermal conductivity
n = normal to interface
P = pressure
Pr = Prandtl number
R = Rayleigh number
Ste = Stefan number
T = temperature
u,v = Cartesian velocity components
V_i = interface velocity
W = width of domain
x,y = Cartesian coordinates
α = thermal diffusivity
β = isobaric compressibility
δ,Δ = change in accompanying variable
γ = nondimensional domain width
Γ = modified diffusion coefficient
ϵ = half-fusion temperature range
λ = latent heat of fusion
ν = kinematic viscosity
ρ = density

Subscripts

d = dynamic
e = east
f = fusion
i = interfacial or dummy variable
i,j = discrete location
ℓ = liquid
n = north
r = reference
s = solid, or south
spec = specified
w = working variable or west
x,y = x or y direction
1,2,3 = solid, melt, or liquid

Superscripts

c = continuity
e,w,n,s,p = geographical molecule location
u,v,p,T = u and v velocity, pressure, temperature
uu,up,vv,vp,TT = equation of first variable, multiplier of second variable
$*$ = nondimensional

Introduction

THE Stefan problem is intrinsically highly nonlinear. This nonlinearity is due to the compatibility constraints imposed at the solidification/melt front and involves the energy fluxes and front propagation velocity at the interface location. However, neither the fluxes, the interface propagation velocity, nor the interface location itself are known a priori. As a result, analytical solutions are available for only a few relatively simple configurations.[1-5] For more realistic problem specifications, discrete methods are required. Traditionally, finite-difference or finite-element methods have been used.

In applications of the enthalpy model[6] to phase change problems, the solution of the algebraic system of equations consumes considerable computing time. This is because complete transient histories are required and Gauss-Siedel iteration or equivalent procedure has been used to solve the equation system. The requirement for an iterative procedure arises from the highly nonlinear character of the interface constraint.[7] In the enthalpy method, the interface location is not tracked explicitly, and its location can be resolved only to within one mesh spacing. The interface nonlinearity, then, appears in the enthalpy model in the form of a highly nonlinear equation of state relating enthalpy to temperature. In addition, this nonlinear behavior is concentrated within the immediate vicinity of the phase change interface and is extremely difficult to accommodate.[8] This is further augmented in problems for which more than one phase interface must be accommodated. Williams and Curry[9] presented a more implicit procedure for the solution of the algebraic equation system for the case of one-dimensional phase change energy transport. Extension of their procedure to more than one space dimension does not appear possible.[10] Since the majority

Received March 29, 1989; revision Sept. 11, 1989.

*Professor, Mechanical Engineering. Member AIAA.

of problems of practical importance involve two or three space dimensions, this is a serious disadvantage. Samonds et al.[11] developed an implicit-explicit, time-stepping algorithm for finite-element analysis, but their model did not include convection.

The numerical solution of solid/liquid phase change problems has been considerably simplified and the associated costs dramatically reduced due to a method by Schneider and Raw[12] for one-dimension problems. This procedure has also been employed in two dimensions by Raw and Schneider[13] with cost reductions comparable to those for the one-dimensional situation, typically two orders of magnitude. All of the preceding methods and applications, however, have included only conduction as the energy transport mode without regard for buoyant convection. In practice, it is frequently this convective motion itself which is the dominant energy transport mechanism. As such, it is crucial that this predictive capability be available in a computational scheme.

There has been little work published in which free convection is included in the model. Recently, Gadgil and Govin,[14] Ho and Viskanta,[15] Yoo and Rubinsky,[16] and Morgan[17] have presented such models. However, all quote extremely high computational times, which is a prime reason for the scant treatment of this problem. Ho and Viskanta,[15] for example, quote run times of 50,000 central processing unit (CPU) s for a single transient evolution using a CDC 6500 installation. This is clearly an exorbitant amount of computing time for their mere 13×21 grid and is the reason that only two simulations were provided. Yoo and Rubinsky[16] and Morgan[17] do not make comparisons with experimental data.

In the present paper, convergence studies are performed on two problems using a procedure introduced by Schneider.[18,19] The procedure employs an enthalpy-like model and incorporates the two rules of Schneider and Raw.[12] Using the proposed model, in conjunction with a coupled, modified, strongly implicit procedure for the fluid-flow solution, computational times for a complete simulation are reduced to less than 10 min for a 10×10 grid on a VAX/785. This is dramatically less than the 833 min quoted by Ho and Viskanta.[15] As such, this is an important step toward rendering the prediction of phase change problems with free convection practical for use as a design and analysis tool and indeed is partially responsible for permitting this convergence study to be performed.

One of the problems examined in this study is the case in which a rectangular phase change material (PCM) section is heated from both the side and bottom of the container. This is a problem for which the computational model of Ho and Viskanta[15] fails. Excellent agreement of the current predictions with experimental data is achieved for both test cases considered.

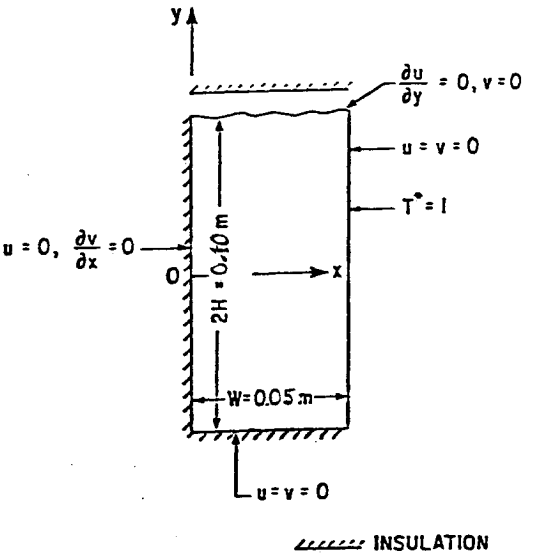

a)

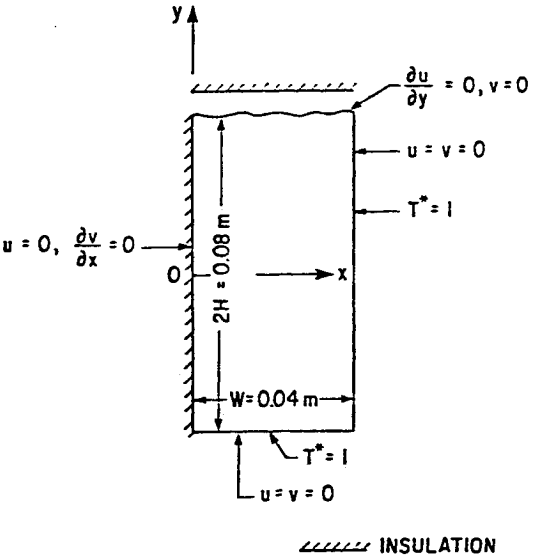

b)

Fig. 1 Problem geometry: a) adiabatic lower surface and b) isothermal lower surface.

Formulation of the Problem

The problems examined in this study correspond to thermal energy transport within a rectangular enclosure in which a PCM undergoes phase transition as its fusion temperature is traversed. The cavity has a height of $2H$ and a width of W. Schematically, the problem geometry is that shown in Fig. 1. The surface at $y = +H$ is a free surface exposed to an air layer bounded by insulation. The boundary defined by $x = 0$ is a surface of symmetry and has zero temperature gradient, zero velocity, and zero tangential shear. The surfaces defined by $x = W$ and $y = -H$ are fixed surfaces and therefore have zero normal and tangential velocity prescribed. The temperature along the boundary defined by $x = W$ is prescribed, and the thermal condition at the boundary $y = -H$ takes on two different prescriptions depending on the case considered. These are:

1) Problem 1: temperature gradient of zero—insulated condition.

2) Problem 2: temperature prescribed to be the same value as that at $x = W$.

The preceding correspond to those examined experimentally by Ho.[20]

The following nondimensional variables are introduced for this problem:

$$x^* \equiv x/H, \quad y^* \equiv y/H, \quad u^* \equiv u/u_0, \quad v^* \equiv v/u_0, \quad P_d^* \equiv \frac{P_d}{P_0}$$

$$e^* \equiv \frac{e - e_{\text{ref}}}{\Delta e_{\text{ref}}}, \quad T^* \equiv \frac{T - T_{\text{ref}}}{\Delta T_{\text{ref}}}, \quad F_0 \equiv \frac{t}{t_0} \tag{1}$$

Properties are normalized by liquid values and reference values are given by

$$u_0 \equiv \frac{\alpha_l}{H}, \quad P_0 \equiv \rho_l u_0^2, \quad t_0 \equiv \frac{L^2}{\alpha_l}, \quad e_{\text{ref}} \equiv e_f, \quad T_{\text{ref}} \equiv T_f$$

$$\Delta e_{\text{ref}} \equiv c_l \Delta T_{\text{ref}} \tag{2}$$

The pressure P is decomposed as

$$P = P_d - \rho_0 g h \tag{3}$$

where h is vertical distance. The governing equations representing conservation of mass, momentum, and energy can then be written in nondimensional form as the following, considering incompressible liquid PCM and employing the Boussinesq approximation for the buoyancy terms.

$$\frac{\partial}{\partial x^*}(u_l^*) + \frac{\partial}{\partial y^*}(v_l^*) = 0 \tag{4}$$

$$\frac{\partial}{\partial Fo}(u_l^*) + \frac{\partial}{\partial x^*}(u_l^* u_l^*) + \frac{\partial}{\partial y^*}(v_l^* u_l^*) = -\frac{\partial P_d^*}{\partial x^*} + Pr_l \times \left[\frac{\partial}{\partial x^*}\left(\frac{\partial u^*}{\partial x^*}\right) + \frac{\partial}{\partial y^*}\left(\frac{\partial u^*}{\partial y^*}\right)\right] - Pr_l Ra_l \times \frac{g_x}{g}(T^* - T_0^*) \tag{5}$$

$$\frac{\partial}{\partial Fo}(v_l^*) + \frac{\partial}{\partial x^*}(u_l^* v_l^*) + \frac{\partial}{\partial y^*}(v_l^* v_l^*) = -\frac{\partial P_d^*}{\partial y^*} + Pr_l \times \left[\frac{\partial}{\partial x^*}\left(\frac{\partial v^*}{\partial x^*}\right) + \frac{\partial}{\partial y^*}\left(\frac{\partial v^*}{\partial y^*}\right)\right] - Pr_l Ra_l \frac{g_y}{g}(T^* - T_0^*) \tag{6}$$

$$\frac{\partial}{\partial Fo}(e_l^*) + \frac{\partial}{\partial x^*}(u_l^* e_l^*) + \frac{\partial}{\partial y^*}(v_l^* e_l^*) = \frac{\partial}{\partial x^*}\left(\frac{\partial T^*}{\partial x^*}\right) + \frac{\partial}{\partial y^*}\left(\frac{\partial T^*}{\partial y^*}\right) \tag{7}$$

$$\frac{\partial}{\partial Fo}(\rho_s^* e_s^*) = \frac{\partial}{\partial x^*}\left(k_s^* \frac{\partial T_s^*}{\partial x^*}\right) + \frac{\partial}{\partial y^*}\left(k_s^* \frac{\partial T_s^*}{\partial y^*}\right) \tag{8}$$

In the preceding, it is assumed that the velocity of the solid PCM is zero. The two parameters appearing in these equations are the Prandtl number and the Rayleigh number.

$$Pr_l \equiv \frac{\nu_l}{\alpha_l}, \qquad Ra_l \equiv \frac{\beta g H^3 \Delta T_{\text{ref}}}{\nu_l \alpha_l} \tag{9}$$

However, the parameter ΔT_{ref} in the Rayleigh number has not yet been established. This is effected through boundary conditions; however, the interfacial constraints must also be applied.

With regard to the interface constraints, continuity of temperature requires that

$$T_l^*|_i = T_s^*|_i = T_f^* = 0 \tag{10}$$

Conservation of energy must also be enforced across the interface. With reference to Fig. 2, conservation of energy applied to an interfacial surface element results in the requirement that

$$-\left.\frac{\partial T_l^*}{\partial n^*}\right|_i = -k_s^* \left.\frac{\partial T_s^*}{\partial n^*}\right|_i + \frac{\rho_s^* V_i^*}{Ste} \tag{11}$$

where the Stefan number is defined as

$$Ste \equiv \frac{c_l \Delta T_{\text{ref}}}{\lambda}$$

Boundary conditions required to complete the mathematical description are given below.

$$x^* = 0; \quad u^* = 0, \quad \frac{\partial v^*}{\partial x^*} = 0, \quad \frac{\partial T^*}{\partial x^*} = 0 \tag{13}$$

$$y^* = -1; \quad u^* = 0, \quad v^* = 0, \quad \frac{\partial T^*}{\partial y^*} = 0 \text{ or } T^* = 1 \tag{14}$$

$$y^* = +1; \quad \frac{\partial u^*}{\partial y^*} = 0, \quad v^* = 0, \quad \frac{\partial T^*}{\partial y^*} = 0 \tag{15}$$

$$x^* = \gamma, \quad u^* = 0, \quad v^* = 0, \quad T^* = 1 \tag{16}$$

where $\gamma \equiv W/H$ and where

$$\Delta T_{\text{ref}} \equiv T_{\text{spec}} - T_f \tag{17}$$

has been introduced with T_{spec} being the specified value of temperature at the right-most surface.

The equation of state will be introduced when the numerical procedure is discussed. For purposes of this paper, the property values of the PCM are independent of its phase. Thus

$$k_s^* \simeq c_s^* \simeq \rho_s^* \simeq 1 \tag{18}$$

The functional dependence of the temperature distribution then takes the form

$$T^* = T^*(x^*, y^*, Fo, \gamma, Pr, Gr, Ste) \tag{19}$$

Numerical Formulation

In this section the numerical procedure employed to solve the phase change problem including free convection is described. In order to include the free convection, the equations of mass and momentum must be solved in addition to the energy equation. Further, the nonlinearity inherent in the interface constraints renders the energy equation extremely difficult to solve even for the case of pure diffusive transport.

The finite-difference method is used in the present work employing the staggered mesh commonly used for fluid-flow

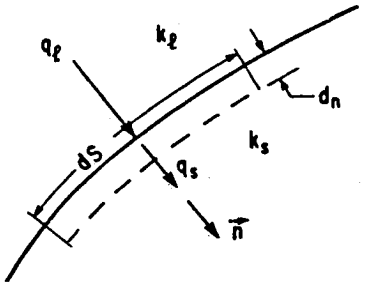

Fig. 2 Interface energy balance.

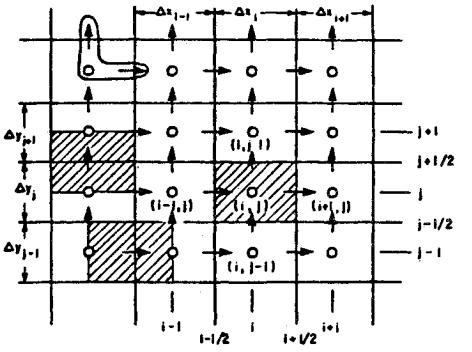

Fig. 3 Finite-differenced mesh.

computation as illustrated in Fig. 3. Pressure and temperature variables are stored at the indicated "nodes," and the u and v velocity components are stored at the faces of these control volumes.

The representation of the continuity equation is obtained by performing a mass balance on continuity control volumes, those having pressure nodes at the control volume centers. The discrete continuity equation, for incompressible flow, has the form, with reference to Fig. 3, given by

$$A^{cu,e}u^*_{i,j} + A^{cu,w}u^*_{i-1,j} + A^{cv,n}v^*_{i,j} + A^{cv,s}v^*_{i,j-1} = 0 \quad (20)$$

The discrete x-momentum equation, for example, is given in the form

$$A^{uu,w}u^*_{i-1,j} + A^{uu,s}u^*_{i,j-1} + A^{uu,p}u^*_{i,j} + A^{uu,e}u^*_{i+1,j} + A^{uu,n}u^*_{i,j+1} + A^{up,w}p^*_{i,j} + A^{up,e}p^*_{i+1,j} = b^u \quad (21)$$

The coefficients in this equation are obtained using the procedure outlined by Patankar.[21] In particular, the momentum flows are evaluated using the power law approximation to the locally one-dimensional, advection-diffusion problem. The central coefficient $A^{uu,p}$ is obtained from

$$A^{uu,p} = -(A^{uu,w} + A^{uu,s} + A^{uu,e} + A^{uu,n}) + C^u \quad (22)$$

where

$$C_V = \rho^*(\delta x^*)_e \Delta y^*_j / \Delta Fo \quad (23)$$

and where (δx^*_e) is the x dimension of the momentum control volume. The source term of Eq. (21) includes the buoyancy driving force term and is given by

$$b^u = -Pr_l Ra_l \frac{g_x}{g}(T^*_{i,j} - T^*_0)(\delta x^*)_e \Delta y^*_j + C^u u^{*0}_{i,j} \quad (24)$$

In a similar fashion, the discrete representation of the y-momentum equation can be determined

$$A^{vv,w}v^*_{i-1,j} + A^{vv,s}v^*_{i,j-1} + A^{vv,p}v^*_{i,j} + A^{vv,e}v^*_{i+1,j} + A^{vv,n}v^*_{i,j+1} + A^{vp,s}p^*_{i,j} + A^{vp,n}p^*_{i,j+1} = b^v \quad (25)$$

where

$$C_u = \rho^*(\delta x^*)_e \Delta y^*_j / \Delta Fo \quad (23)$$

with C^v and b^v given by

$$C^v = \rho^* \Delta x^*_i (\delta y^*)_n / \Delta Fo, \quad (27a)$$

$$b^v = -Pr_l Ra_l \frac{g_y}{g}(T^*_{i,j} - T^*_0)\Delta x^*_i (\delta y^*)_n + C^v v^{*0}_{i,j} \quad (27b)$$

The thermal energy equation is treated analogously to the momentum equations. However, the energy equation contains a mixture of internal energy and temperature terms; internal energy is stored and convected while the temperature is diffused. This mixture is resolved through the equation of state.

Following Schneider,[12,13] the internal energy is approximated by enthalpy and a piecewise linear equation of state is used to effect complete passage from solid, through "melt," to liquid. For this purpose, a phase transition, or melt, phase is introduced. Denoting the solid, phase transition, and liquid phases by subscripts 1, 2, and 3, respectively, the equation of state is given by a single general equation

$$h^* = h^*_{f,i} + c^*_{p,i}(T^* - T^*_{f,i}), \qquad i = 1,2,3 \quad (28)$$

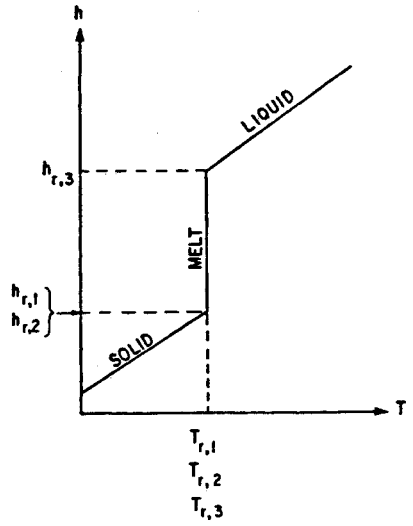

Fig. 4 Equation of state.

where the subscript f denotes a reference value. This reference value is chosen for convenience, since only changes in energy or enthalpy are required, but the constraint is required when dealing with the PCM that the equation of state must be continuous.

One consistent set of reference values, as illustrated in Fig. 4, is given by

$$h^*_{f,1} = 0 \qquad T^*_{f,1} = -\epsilon \qquad c^*_{p,1} = c^*_s$$

$$h^*_{f,2} = 0 \qquad T^*_{f,2} = -\epsilon \qquad c^*_{p,2} = \frac{0.5}{Ste \cdot \epsilon} + \frac{1 + c^*_s}{2}$$

$$h^*_{f,3} = 1/Ste \qquad T^*_{f,3} = +\epsilon \qquad c^*_{p,3} = 1 \quad (29)$$

where ϵ is a small value, typically of order 10^{-4}, whose influence is representation of phase transition by a large specific heat over a negligibly small temperature range. In the discrete problem, therefore, the Stefan number appears in the property relations, whereas it appears in the continuum problem in the interface constraints.

The generalized equation of state can be rewritten in the more compact form

$$h^* = h^*_{w,i} + c^*_{p,i}T^* \quad (30)$$

where

$$h^*_{w,i} = h^*_{f,i} - c^*_{p,i}T^*_{f,i} \quad (31)$$

Using the preceding form for the equation of state, it is possible to express the energy equation in a form which is primarily dependent on temperature. This equation has the form

$$A^{TT,w}T^*_{i-1,j} + A^{TT,s}T^*_{i,j-1} + A^{TT,p}T^*_{i,j} + A^{TT,e}T^*_{i+1,j} + A^{TT,n}T^*_{i,j+1} = b^T \quad (32)$$

where

$$A^{TT,p} = -[A^{TT,w} + A^{TT,s} + A^{TT,e} + A^{TT,n}] + C^T c^*_{p,i}|_{i,j} \quad (33)$$

and where the evaluation of the A^{TT} terms, representing sensible energy flows, has been done using the methods of Patankar[21] with the effective coefficient for diffusion given by

$\Gamma^* = k^*/C^*_{p,i}$ evaluated at the appropriate location. The C^T and b^T in the preceding are given by

$$C^T \equiv \frac{\rho^* \Delta x^*_i \Delta y^*_j}{\Delta Fo} \tag{34a}$$

$$b^T = C^T c^*_{p,i}|_{i,j} T^{*0}_{ij} - C^T, (h^*_{w,i} - h^{*0}_{w,i})|_{i,j} \tag{34b}$$

It is noted that the form of the equation given by Eq. (32), with Eqs. (34), involves relatively few occurrences of $h_{w,i}$, even though these values appear in every convective energy transport term of the energy balance. This is a result of invocation, at discrete level, of the continuity equation. Each convection term leads to a mass flow times reference enthalpy contribution and it is further noted that the assumption, presented earlier, has been made that the velocity of nonliquid regions of the domain is identically zero. Therefore, the only nonzero velocity contributions are due to liquid flow, and as these flows have identical reference enthalpies, their influence cancels exactly through conservation of mass. The net convection energy transport is then only the sensible component. However, the primary influence of convection, that of transporting highly energetic liquid to the phase change interface, where it can contribute significantly to the phase front erosion through melting, has been retained in the model.

Numerical Solution Considerations

In phase change energy transport, the entire problem is temporally evolutionary with all transient details important to the problem resolution. Consequently, it is essential that sufficiently small time steps be employed such that changes in the temperature field or in the fluid flowfield from time step to time step significantly reduce the nonlinear coupling between the energy and fluid-flow equations. This realization is used to advantage in the present solution procedure to preclude energy-fluid flow equation iteration and to preclude the nonlinear iteration normally required of the fluid-flow equations themselves. The justification for such a procedure is the use of sufficiently small time steps in the transient evolution. The remedy for inaccurate computations from this source, therefore, is to further decrease the time step. The algorithmic simplifications that result from such a procedure are significant and fully justify use of the procedure.

The strategy for the transient evolution of the fluid flow and temperature fields, then, is that depicted by the following sequence of computations for advancement over a single time step.

1) Enter the new time level with velocity and temperature fields from the previous time step.

2) Using the proceding, coefficients are calculated for the fluid-flow equation system.

3) The thereby linearized, but highly coupled, mass-momentum equation system is then solved.

4) These new velocities are used in the coefficient calculation for the energy equation.

5) The thereby linearized energy equation is solved.

6) As a result of steps 3 and 5, new time-level predictions are available for the velocity, pressure, and temperature fields. Enthalpy and melt fraction predictions can then be determined.

7) The time level is advanced, and the procedure is repeated from step 1.

The preceding procedure is noniterative and requires fixed computational tasks for each time step, each of which, by itself, is nontrivial. The procedure employs the evolutionary character of the problem as a feedback mechanism to accomplish the normally required interequation iteration. The preceding list presents, in an algorithmic sequence, the overall strategy employed for each time step. Some comments are still necessary.

The solution of the mass-momentum equation system is a significant task in the overall algorithm. The method employed for the fluid-flow solution is the coupled modified strongly implicit procedure of Zedan and Schneider.[22] In this procedure, a derived equation is used for pressure (replacing the continuity equation) in a strongly implicit iteration algorithm. This derived equation renders the equation system more diagonally dominant than the original and enhances the iterative convergence. It is noted, however, that this pressure equation is derived in such a manner that when the solution is obtained, the original continuity equation is indeed satisfied. Whereas this solution procedure has slightly higher computational costs than do some other optimized procedures, the costs of these alternative procedures are relatively sensitive to the (many) solution procedure parameters, and effecting the optimization frequently exceeds the actual costs of solution. Conversely, the coupled modified strongly implicit procedure has relatively few parameters with procedural performance more weakly dependent on the remaining parameters.

With regard to the nonlinearity of the Stefan problem, an extension has been made to a procedure developed by the author for one-dimensional, diffusion-dominated phase change energy transport[12] to the multidimensional configuration.[13] This has been incorporated into the free convective energy transport code. The procedure still requires iteration to resolve the nonlinearity, but it is of a significantly different form that is closer to a predictor-corrector method than a point relaxation method. Each time step calculation proceeds as follows.

1) As a guess, the phase distribution of new time levels is assumed the same as the current level.

2) On this assumption, the energy equation is solved directly.

3) The new tentative temperature solution yields a new tentative phase distribution. The guessed and tentative phase distributions are compared, and by applying two rules, presented below, to the tentative phase distribution, a modified guess for the new phase distribution is generated.

4) Steps 2 and 3 are repeated until the modified and tentative phase distributions agree.

This calculation is contingent on two fundamental rules. Experience has shown that when the time interval is large enough to move the front by one control volume boundary per time step, typically only two or three iterations of steps 2 and 3 are required. If the conditions are such that the front does not cross a control volume boundary, then the first guess is correct, and only one iteration is required. This has been shown to lead to a drastic reduction in execution cost.[12,13] The two rules that enable this cost reduction follow directly from enforcing the correct physical behavior if the iterations are viewed as a transient evolution.

Rule 1: In one iteration, the modified guess phase for a control volume can only change from its previous iteration value by one. Thus if the tentative phase is liquid and the guessed phase was solid, the modified guess will be restricted to melt as a maximum excursion from its present phase.

Rule 2: If the phase states of the previous iteration for a control volume and all of its neighbors were the same, then the modified guess for the phase of the control volume in question must not be changed. For example, if the tentative phase of a control volume is liquid but the previous guess for it and all of its neighbors was solid, then the modified guess will remain the solid phase.

Rule 1 enforces the physical requirement that in changing from solid to liquid, or vice versa, a phase must pass through the melt phase. If this is not satisfied, the system will not have acknowledged the enthalpy difference that exists between the solid and liquid states. Rule 2 is a statement that enforces the physical requirement that a phase change in one region cannot occur without a neighboring region having changed phase first. This, of course, is restricted to zero internal source strength situations but can readily be modified.

Subject to the assumed phase distribution, it is still required

to obtain the solution to the energy-equation algebraic system. If the correct phase distribution within the PCM is known, or a suitably fixed distribution is assumed as per the preceding iteration sequence, the energy-equation discretization represents a linear algebraic system in terms of the control volume temperatures for which a solution is required. For small problem sizes, a direct solution procedure may be employed. However, as the problem size grows, the continued use of a direct solver rapidly becomes prohibitively expensive, and iterative methods for the solution of the linearized problem must be employed. The method employed here is the modified strongly implicit procedure of Schneider and Zedan.[23]

Comparison with Experiment

The computational model was first executed for the problem geometry of Fig. 1a. This configuration corresponds to that examined experimentally and numerically by Ho and Viskanta,[15] although the numerical work of Ho and Viskanta was limited to a single computational run. The PCM is *n* octadecane with a corresponding Prandtl number of $Pr_\ell = 50$. The Rayleigh number, based on the surface temperature-fusion temperature difference and on the half height of the cell, is 1.57×10^7. The experiment was initiated with zero subcool, solid-phase conditions throughout, and this was simulated in the numerical experiments with an initial nondimensional subcool of -0.002. The range of nondimensional temperature is from 0 to 1. The actual cavity dimensions of the Ho and Viskanta[15] experiment were 0.10 m total height and 0.05 m width. It is noted that the paper by Ho and Viskanta implies a cell height of 0.13 m, but the actual height of 0.10 m is obtained from the thesis by Ho.[20]

On the basis of several test runs, it was determined that a nondimensional time step determined according to $Ste \cdot \Delta Fo = 10^{-4}$ provided accurate temporal resolution at early time. At later times, when the melt had more fully penetrated the PCM, this was gradually relaxed to $Ste \cdot \Delta Fo = 5 \times 10^{-3}$. Four different mesh discretizations were employed. These correspond to a 10×10 mesh (8×8 interior control volumes), a 20×20 mesh (18×18), a 40×20 mesh (38×18), and a 60×30 mesh (58×28). The experimental data of Ho and Viskanta[15] extend only to a 25% melt fraction limit, and the numerical simulations fully capture the physics of this problem.

Results for this problem obtained from the 60×30 mesh are presented in Fig. 5 as velocity vector diagrams with mirror image representation of the isotherms. In succession, these plots form the melting history profile for the problem. In all of the plots shown here, the minimum and maximum isotherms correspond to values of 0 and 1, respectively, for nondimensional temperature. For small Fo, there is relatively little liquid-phase PCM and the fusion isotherm, $T^* = 0$, corresponding to the phase-front interface, is nearly vertical. It is also clear from the figure that a large recirculation cell has been established within the liquid PCM. At $Fo = 0.09$, the liquid region has expanded while the interfacial front is still very nearly vertical. The strength of the recirculation has increased, and it is also observed that there are two recirculation cells beginning to emerge within a large overall recirculation cell. That is, part of the downward flow near the cold-phase front is "stripped off" and moves up, and a similar phenomenon occurs at the hot wall. This occurs at approximately 40% distance from the bottom surface. However, this effect is relatively weak. It is noted that recirculation strength increases throughout the entire melt and that the velocity vectors are scaled to the maximum for that particular time. Thus the growth in convection strength is not exhibited from figure to figure in the sequence. Rather, the relative spatial convection strength within a specific plot is preserved.

For $Fo = 0.13$, the weak secondary cells have coalesced, and a single recirculation cell exists. It is evident, however, that the recirculation in the top left region of the liquid is becoming considerably more vigorous as melting is proceeding. It is also evident that the interfacial front is beginning to depart more noticeably from its almost vertical configuration and that increased erosion of the melt front is occurring near the top of the PCM as is expected. For $Fo = 0.17$, the weak secondary recirculation zones are no longer present. The 0.6 isotherm displays strongly in this figure the "temperature inversion" phenomenon, which occurs in strongly convecting buoyancy driven flows. The strong convection of warm fluid proceeds up along the heated wall and is deflected to the left and then down the phase-front interface side of the recirculation cell.

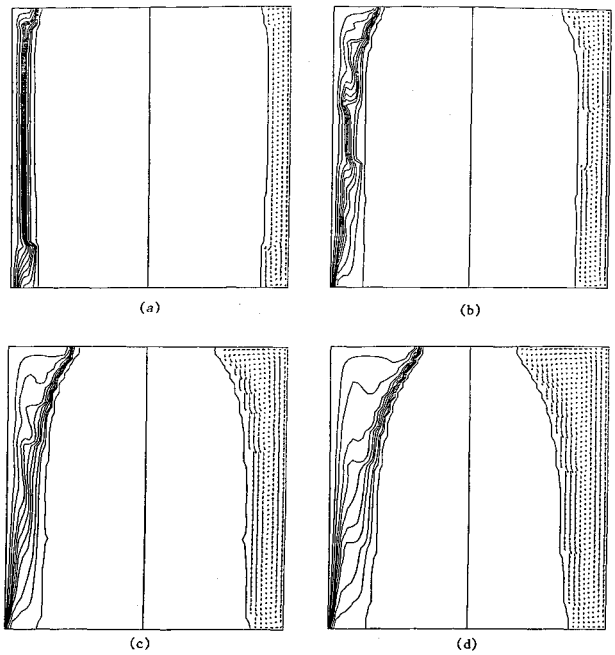

Fig. 5 Problem 1 velocity vector and isotherms results: a) $Fo = 0.05$, b) $Fo = 0.09$, c) $Fo = 0.13$, d) $Fo = 0.17$.

Clearly from the preceding descriptions, the phase-change melting problem is a dynamic process. As time progresses through the melting evolution, significant changes occur in the temperature field, the melt front configuration, and the velocity distribution and flow pattern. Although the interpretations given to the various figures examined are physically self-consistent, such self-consistency does not guarantee or imply accuracy of the predictions. A more quantitative evaluation, through comparison of the computed melt fraction history with the experimentally measured melt fraction history reported by Ho and Viskanta[15] and by Ho,[20] is provided below.

The predicted melt fraction histories will be compared with the experimental melt fraction history reported by Ho and Viskanta[15] and by Ho.[20] Since experimental data are available only for melt fractions less than approximately 25%, the comparisons will be restricted to this part of the evolution. Four separate computational runs were executed for this purpose as was mentioned earlier.

The results of the four computations are compared with the experimental data and with the predictions of Ho and Viskanta[15] in Fig. 6. The 10×10 grid predictions are clearly below both the data and the Ho and Viskanta predictions. This is consistent since it is expected that coarse grid computations for this problem will underpredict the melting rate. The 20×20 grid predictions are also below the experimental data and correspond closely to the Ho and Viskanta 13×21 (horizontal $\times$ vertical), transformed, liquid domain predictions. It is noted that Ho and Viskanta attributed their underpredictions to the inability of their model to account for the "flooding" that occurs over the top surface as a result of volumetric expansion of the PCM upon melting and to the neglect of

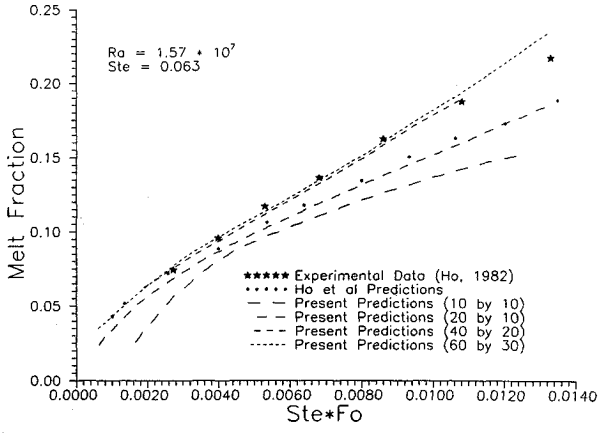

Fig. 6 Melt fraction and convergence study for problem 1.

surface velocities normal to the phase front resulting from the same volumetric expansion influences.

The present 40×20 predictions are rather startling. With this increased resolution, the predictions are in excellent agreement with the experimental data. It is observed that the dependence of the prediction accuracy on grid size and spatial resolution is relatively severe. The finest grid of 60×30 provides results for the melt fraction that are essentially coincident with the 40×20 results. This therefore provides excellent validation of the prediction computations and of the modeling of the problem physics.

Computational run times for the preceding problem, as an entire transient evolution, remain high. However, they are significantly reduced from that reported in the work of Ho and Viskanta.[15] In their work a time per run of 50,000 CPU s (i.e., 13.9 h) was reported for a CDC 6500 installation. In comparison, the present procedure required only about 3 h for the finest grid on a CDC 6600 installation. Although these times are indeed still large, they represent cost reductions estimated to be a factor of 30 for the same level of discretization. Such a cost reduction is substantial.

The computational model was also executed for the problem geometry of Fig. 1b. This configuration corresponds to that examined by Ho.[15] The PCM is *n* octadecane with a corresponding Prandtl number of $Pr_\ell \approx 50$. The Rayleigh number, based on the surface temperature-fusion temperature difference and on the half height of the cell, is 1.82×10^7. The Stefan number for this problem is $Ste = 0.133$. The initial subcool of the PCM was nonzero and corresponds to an initial nondimensional temperature within the solid of $T^*_{\text{init}} = -0.2$. The range of nondimensional temperature is from 0 to 1. The dimensions of the PCM were 0.08 m total height and 0.04 m width. For this problem, however, the computational model of Ho and Viskanta[15] fails and is unable to provide predictions for comparison purposes. Thus, there are no available computational results for comparison with the present results. Comparisons are only made to the actual experimental results of Ho.[20]

On the basis of several test runs, it was determined that a nondimensional time step determined according to $Ste\cdot\Delta Fo = 10^{-4}$ provided accurate temporal resolution at early time. At later times, when the melt has more fully penetrated the PCM, this was gradually relaxed to $\text{Ste}\cdot\Delta Fo = 5\times10^{-3}$. In the numerical computations, different mesh sizes and different levels of subcool were examined. The mesh size/subcool combinations employed are 20×20 mesh with subcool of -0.2, 20×20 mesh with subcool of -0.002, 40×40 mesh with subcool of -0.2, and 60×60 mesh with subcool of -0.2.

Results for this problem obtained from the 60×60 mesh and with $T_{\text{init}} = -0.2$ are presented in Fig. 7 as velocity vectors

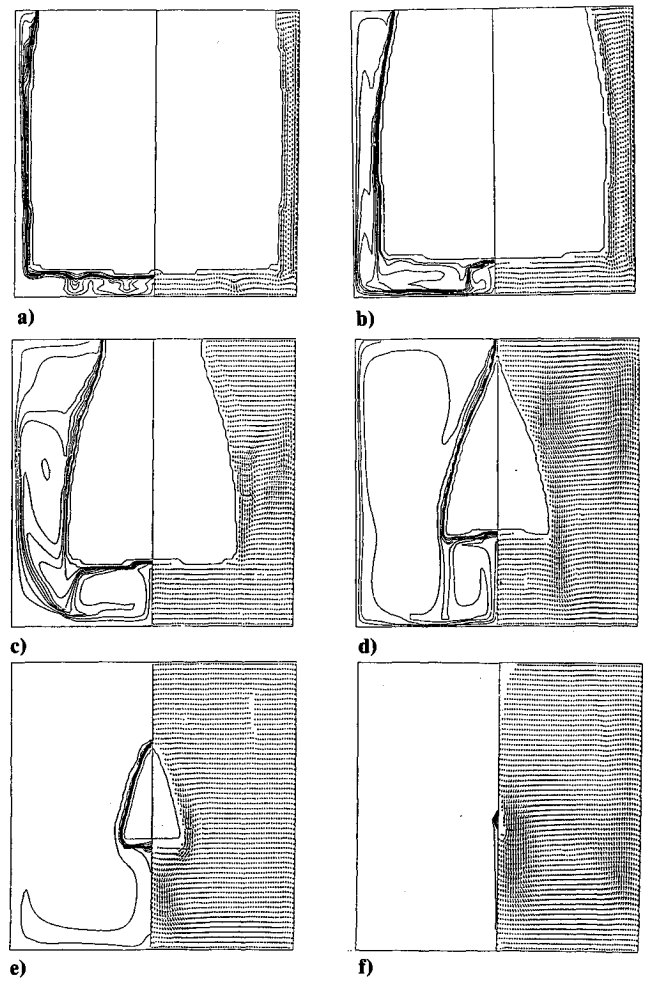

Fig. 7 Problem 2 velocity vector and isotherm results: a) $Fo = 0.050$, b) $Fo = 0.100$, c) $Fo = 0.200$, d) $Fo = 0.300$, e) $Fo = 0.350$, f) $Fo = 0.400$.

with mirror image isotherm representation. In succession, these plots form the melting history profile for the problem. In all of the plots shown here, the minimum and maximum isotherms correspond to values of 0 and 1, respectively, for the nondimensional temperature. For $Fo = 0.05$, there is a relatively small amount of molten PCM. A large recirculation cell is in existence along the right boundary with two minor recirculation cells along the right surface. The fusion front is relatively straight and vertical along this boundary. Along the bottom boundary, however, there exist four recirculation cells exclusive of that occurring at the right-most boundary. These recirculation cells result in a relatively irregular fusion front due to the differing erosion rates that would result between upward-directed and downward-directed portions of the convection cells. It is further noted that the 20×20 coarse mesh did not capture these smaller recirculation cells.

For $Fo = 0.1$, it is seen that there is an increased amount of molten PCM. Further, the increased erosion of the fusion front at the top-right corner of the PCM is apparent. This results from the convection of warm liquid PCM upward along the right-most boundary being deflected at the top free surface and discharging its energy to the solid PCM and thereby causing additional melting at the top region of the solid PCM. As the liquid loses energy in this fashion, as it falls down the fusion boundary, less melting occurs due to the decreased available energy for the latent heat transformation. Along the lower surface, there now exist only two recirculation cells. These lower-surface recirculation cells are thus beginning to coalesce.

For $Fo = 0.2$, the preferential erosion of the top-right boundary is more apparent as a result of the increased time for this preferential erosion to occur. The increased width of the liquid layer at the right surface has resulted in a single, large recirculation cell in this region. In examining the shape of the isotherms for this plot, the inversion phenomenon characteristic of free convection motion has begun to emerge. It can be seen that a "finger" of cold fluid is rising upward near, but not adjacent to, the fusion front. This behavior is typical of high Rayleigh number, free-convection recirculation. At the bottom surface, a single recirculation cell now exists with the previous smaller cells having coalesced to form this larger cell. Further, the downward motion of both the right wall cell and the bottom surface cell coincide at the lower right corner, and a cold finger of liquid is seen to be swept into the surrounding liquid from this lower, right corner. It can be seen, at its tip, to be spreading in directions coincident with both recirculation cells.

For $Fo = 0.30$, the characteristics are similar to those just described but have an increased volume of liquid PCM. The last two parts of the figure show completion of the evolution to a state of complete melt. The primary departure from the just-described flow patterns is that the recirculation in the lower-left corner is no longer present.

It is further noted, in conjunction with the melt fraction histories to be presented, that the shape of the fusion front is very closely representative of that reported by Ho.[20] The shapes observed by Ho[20] displayed a curve toward the center at the top-right surface of the solid rather than the perpendicular configuration indicated here. The perpendicular intersection of the fusion front with the top surface is dictated by the imposition of a zero temperature gradient at this surface. Further, in the actual experiment, the PCM expands upon melting and occupies a larger volume than the comparable mass of solid PCM. This results in some of the liquid PCM flowing over the top of the solid and initiating a certain amount of melt from the top of the solid due to the presence of molten PCM on this surface. Excepting this minor variation, the agreement of the predicted fusion front shapes with those observed by Ho[20] is excellent.

The predicted melt fraction histories are also compared with the experimental melt fraction history reported by Ho.[20] Four separate computational runs are reported for this purpose: 1) 20×20 mesh with -0.2 initial subcool, 2) 20×20 mesh with zero initial subcool, 3) 40×40 mesh with -0.2 initial subcool, and 4) 60×60 mesh with -0.2 initial subcool. The results of these computations are compared with the experimental data of Ho[20] in Fig. 8. The first computational run was conducted for the 20×20 mesh with an initial solid subcool nondimensional temperature of -0.2. It is seen that these predictions at low time overpredict the experimental melt fraction, whereas at large time these predictions significantly underpredict the melt fraction history. The early time overprediction can be explained by the coarseness of the mesh employed. The Dirichlet boundary condition on temperature at the diabatic surfaces causes the control volumes adjacent to the boundary to immediately assume a nonzero melt fraction. This is a result of the linearity of the profile at the boundary at early times causing all control volumes immediately adjacent to the boundary to take on a finite melt fraction.

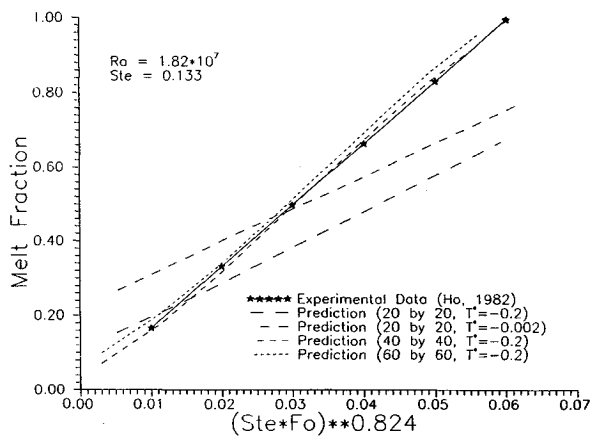

Fig. 8 Melt fraction and convergence study for problem 2.

The underprediction of the melt fraction at large time can also be attributed to the coarseness of the mesh. The coarse mesh limits the extent to which the free convective fluid motion can transport thermal energy. Indeed the slope of the melt fraction history is significantly underpredicted and is attributed to the underprediction of the fluid-flow velocities due to the coarse mesh. The influence of initial subcool was examined by running the same mesh with an initial subcool nondimensional temperature in the solid in -0.002 (essentially zero). The primary impact of the higher initial temperature is to raise the curve to that shown in the figure. The slope of the curve remains essentially as before with overprediction of melt fraction at small time and underprediction at large time.

The results corresponding to an initial subcool of -0.2 but for a 40×40 computational mesh are also shown in the figure and show a dramatic departure from the previous, coarser mesh, results. First, the behavioral change in the predicted melt fraction history is markedly different from that obtained using the 20×20 mesh. Second, the agreement of the computational predictions with the experimental data of Ho[20] is excellent throughout the entire melting history. Finally, the 60×60 mesh results are also shown in the figure and are only slightly displaced from the 40×40 results. This very accurate prediction of the fine grid simulation provides excellent validation of the code and modeling of the problem physics.

Conclusions

A numerical procedure has been presented for the computation of phase-energy transport including free-convection motion. In the model, the mass and momentum equations are solved in addition to the thermal energy equation. An enthalpy-like model is employed in modeling the phase change interface nonlinearity and the procedure for treating this nonlinear problem, advanced previously by Schneider and Raw[12] and Raw and Scheider[13] for diffusion dominated phase change, has been extended to the problem including free-convective motion. A coupled modified strongly implicit procedure has been employed in the solution of the coupled velocity-pressure part of the problem. The velocity of all nonliquid PCM has been assumed to be zero and is consistent with expectations for the particular problem examined.

The particular problems examined are those described by Ho and Viskanta[15] wherein a vertical isothermal boundary interacts with an initially solid PCM being insulated on the other sides and having a free surface at the top. For the second problem, the bottom surface is also isothermal with this small difference providing for a significantly more complex flow and energy transfer phenomenon. The paraffin *n* octadecane was used, with $Pr_l = 50$. Qualitative results have been presented, which show the development of the flowfield within the liquid PCM. The problems were seen to be quite dynamic with several recirculation cells appearing at various stages in the evolution. In addition, quantitative results have been presented in terms of the melt fraction history for both problems. Comparisons of the present predictions with the experimental results of Ho and Viskanta[15] have been presented as well as comparisons with their predictions where applicable. It was observed that the melt fraction results can be relatively sensitive to the level of discretization employed in the problem. The present predictions for problem 1 and for the 20×20 grid are in good agreement with the 20×13 results of Ho and

Viskanta.[15] However, both of these results lie considerably below the experimental data for this problem. The present fine-grid results predict the experimental data remarkably well and are significantly removed from the Ho and Viskanta[15] predictions and from the present coarsest grid results.

The overall success of the present model and the present computational procedure are judged to be excellent. Not only are the predictions in excellent agreement with the experimental data, but, in addition, the cost of the computational predictions are considerably lower (estimated at a factor of 30) than that incurred by the previous computations for this problem.

Acknowledgments

The author acknowledges the financial support of the Natural Sciences and Engineering Research Council of Canada, through an operating grant to the author, and the NASA Langley Research Center, through a contract with the author administered by A. Fripp, Jr. The author thanks K. Wittich for his assistance in performing the computations, and A. Fripp for fruitful discussion of the subject matter. Some of the computations were performed using the NASA Langley Research Center computational facilities.

References

[1]Imber, M., and Huang, P. N. S., "Phase Change in a Semi-Infinite Solid with Temperature Dependent Thermal Properties," *International Journal of Heat and Mass Transfer*, Vol. 16, No. 10, Oct. 1973, pp. 1951–1954.

[2]Chung, B. T. F., and Yeh, L. T., "Freezing and Melting of Materials with Variable Properties and Arbitrary Heat Fluxes," *AIAA Journal*, Vol. 14, No. 3, 1976, pp. 388–390.

[3]Hayashi, Y., Komori, T., and Katayana, K., "Analytical and Experimental Investigation of Self Freezing," American Society of Mechanical Engineers, New York, Paper 75-HT-VV, Jan. 1975.

[4]Zien, T.-F., "Analytical Study of Heat Conduction with Phase Transition," AIAA Paper 76-171, Jan. 1976.

[5]Özişik, M. N., and Uzzell, J. C., "Exact Solution for Freezing Temperature Range," *Journal of Heat Transfer*, Vol. 101, Series C., May 1979, pp. 331–334.

[6]Shamsundar, N., and Sparrow, E. M., "Analysis of Multidimensional Conduction Phase Change via the Enthalpy Model," *Journal of Heat Transfer*, Vol. 97, Aug. 1975, pp. 333–340.

[7]Ronel, J., and Baliga, B. R., "A Finite Element Method for Unsteady Heat Conduction in Materials With or Without Phase Change," American Society of Mechanical Engineers Winter Annual Meeting, New York, Dec. 1979.

[8]Baliga, B. R., personal communication, Aug. 1982.

[9]Williams, S. D., and Curry, D. M., "An Implicit Formulation for the One-Dimensional Two-Phase Multi-Dimensional Stefan Problem," American Society of Mechanical Engineers, New York, Paper 82-HT-21, June 1982.

[10]Williams, S. D., personal communication, June 1982.

[11]Samonds, M. Morgan, K., and Lewis, R. W., "Finite Element Modeling of Solidification in Sand Castings Employing an Implicit-Explicit Algorithm," *Applied Mathematical Modeling*, Vol. 9, June 1985, pp. 170–174.

[12]Schneider, G. E., and Raw, M. J., "An Implicit Solution Procedure for Finite Difference Modeling of the Stefan Problem," AIAA Paper 83-1527, June 1983; also *AIAA Journal*, Vol. 22, No. 11, 1984, pp. 1685–1690.

[13]Raw, M. J., and Schneider, G. E., "A New Implicit Solution Procedure for Multi-Dimensional Modelling of the Stefan Problem," *Numerical Heat Transfer*, Vol. 8, 1985, pp. 559–572.

[14]Gadgil, A., and Govin, D., "Analysis of Two-Dimensional Melting in Rectangular Enclosures in Presence of Convection," *Journal of Heat Transfer*, Series C, Vol. 106, Feb. 1984, pp. 20–26.

[15]Ho, C.-J., and Viskanta, R., "Heat Transfer During Melting from an Isothermal Vertical Wall," *Journal of Heat Transfer*, Series C, Vol. 106, Feb. 1984, pp. 12–19.

[16]Yoo, J., and Rubinsky, B., "A Finite Element Method for the Study of Solidification Processes in the Presence of Natural Convection," *International Journal for Numerical Methods in Engineering*, Vol. 23, 1986, pp. 1785–1805.

[17]Morgan, K., "A Numerical Analysis of Freezing and Melting with Convection," *Computer Methods in Applied Mechanics and Engineering*, Vol. 28, 1981, pp. 275–284.

[18]Schneider, G. E., "Finite Difference Computation of Solid/Liquid Phase Change Energy Transport," AIAA Paper 86-0067, Jan. 1986.

[19]Schneider, G. E., "Computation of Heat Transfer with Solid/Liquid Phase Change Including Free Convection," AIAA Paper 85-0404, Jan. 1985; also *Journal of Thermophysics and Heat Transfer*, Vol. 1, No. 2, 1987, pp. 136–145.

[20]Ho, C. J., "Solid-Liquid Phase Change Heat Transfer in Enclosures," Ph.D. Thesis, Purdue Univ., West Lafayette, IN, Dec. 1982.

[21]Patankar, S. V., *Numerical Heat Transfer and Fluid Flow*, McGraw-Hill, New York, 1980.

[22]Zedan, M. G., and Schneider, G. E., "A Coupled Strongly Implicit Procedure for Velocity and Pressure Computation in Fluid Flow Problems, *Numerical Heat Transfer*, Vol. 8, No. 5, 1985, pp. 559–572.

[23]Schneider, G. E., and Zedan, M. G., "A Modified Strongly Implicit Procedure for the Numerical Solution of Field Problems," *Numerical Heat Transfer*, Vol. 4, No. 1, 1981, pp. 1–19.

[24]Schneider, G. E., "Computation of Heat Transfer with Solid/Liquid Phase Change Including Free Convection," *Journal of Thermophysics and Heat Transfer*, Vol. 1, No. 2, 1987, pp. 136–145.